BNL-222310-2021-JAAM

Coupling CO2 reduction with ethane aromatization for enhancing catalytic stability of iron-modified ZSM-5

Z. Xie

To be published in "JOURNAL OF ENERGY CHEMISTRY"

March 2022

Chemistry Department

Brookhaven National Laboratory

U.S. Department of Energy

USDOE Office of Science (SC), Basic Energy Sciences (BES) (SC-22)

DISCLAIMER

Coupling CO_2 reduction with ethane aromatization for enhancing catalytic stability of iron-modified ZSM-5

Zhenhua Xie,[a,b] Elaine Gomez,[a] Dong Wang,[a] Ji Hoon Lee,[a] Tiefeng Wang,[c] Jingguang G. Chen[a,b,*]

[a] Department of Chemical Engineering, Columbia University, New York, NY 10027, USA

[b] Chemistry Division, Brookhaven National Laboratory, Upton, NY 11973, USA

[c] Department of Chemical Engineering, Tsinghua University, Beijing 100084, Beijing, China

*Corresponding author. E-mail address: jgchen@columbia.edu (J. G. Chen).

Abstract

The shale gas revolution and the carbon-neutrality goal are motivating the landscape toward the synthesis of value-added chemicals or fuels from underutilized ethane with the assistance of greenhouse gas CO_2. Combining ethane aromatization with CO_2 reduction offers an opportunity to directly produce liquid products for facile separation, storage, and transportation. In the present work, Fe/ZSM-5 catalysts showed promise in the simultaneous CO_2 reduction and ethane aromatization at atmospheric pressure and 873 K. The catalysts were further investigated using X-ray diffraction (XRD) and X-ray absorption fine structure (XAFS) measurements under *in-situ* conditions, indicating that most of Fe species existed in the form of Fe oxides and a portion of Fe was incorporated into the ZSM-5 framework generating Lewis acid sites. Both types of Fe species remained almost unchanged under reaction conditions, contributing to an enhanced aromatization activity of Fe/ZSM-5. The effects of CO_2 and steam on the acid sites and in turn aromatization activity were also investigated by transient studies, which exhibited a reversible modification behavior. Moreover, CO_2 was identified to be critical to enhance coke resistance and in turn catalyst stability. This work highlights the feasibility of using CO_2 to assist the upgrading of abundant ethane from shale gas to aromatics over non-precious Fe-based zeolite catalysts.

Keywords: Ethane, CO_2, Aromatization, Fe-modified ZSM-5.

1. Introduction

Anthropogenic CO_2 emission has shown a significant increase in the past few decades, which has been correlated to global climate change and ocean acidification [1,2]. Many approaches have been proposed and exploited towards the reduction of CO_2 emission [1,3,4]. In recent years, employing CO_2 as a reactant or co-reactant to produce value-added chemicals and fuels is widely investigated as a promising approach for CO_2 reduction [5–10]. One of the most practical routes is to combine CO_2 reduction with the catalytic conversion of light alkanes that are abundant in shale gas [11–14]. Ethane is the second-most component in the huge-reserved shale gas (ca. 16.1 quadrillion cubic feet globally) while still underutilized despite its record low price since 1995 [15], thereby offering opportunities to be used as a co-reactant to reduce CO_2.

Currently, the reported routes to react ethane with CO_2 are mainly the dry reforming (DR) of ethane to syngas (CO and H_2) and the oxidative dehydrogenation (ODH) of ethane to ethylene using CO_2 as a soft oxidant [11,16]. Although valuable molecules are produced by DR and ODH of ethane, the separation of gas phase products from the reactants is still challenging. From this perspective, it is highly desirable to develop a tandem reaction to directly produce liquid products from the reaction of ethane and CO_2, which would greatly simplify the separation step and facilitate the production, storage and transportation of liquid products [8].

Aromatization is a potential route that can be integrated ethane upgrading with CO_2 reduction in a single process. Aromatics (*i.e.*, benzene, toluene and xylenes) are the essential building blocks in petrochemical industries and are conventionally produced

from naphtha reforming [17], whereas the naphtha raw materials account for nearly 80% of the production cost [18]. Thus, replacing naphtha with the inexpensive and abundant ethane from shale gas is economically promising. Our previous work has reported the feasibility of coupling CO_2-assisted ODH of ethane to ethylene and aromatization of ethylene, with both reactions occurring at similar temperature and pressure [13]. In addition, carbon deposition on catalysts has been identified as a significant barrier for the practical application of aromatization; in the current case, the co-reactant CO_2 can reduce coke formation *in-situ* via the reverse Boudouard reaction ($CO_2 + C \rightarrow 2CO$), thereby beneficial to catalyst stability.

The production of aromatics from ethane typically proceeds with either the sequential dehydrogenation-oligomerization-cyclization-dehydrogenation route or the hydrocarbon pool (typically at high temperatures) route [19]. Zeolite-based materials have been identified and widely applied for aromatization. Previous studies report that zeolites used for the aromatization of light alkanes (C1-C4) are mostly of the MFI type (e.g., ZSM-5) because of its unique channel dimension, shape selectivity and acid properties [20]. However, the pure HZSM-5 zeolite with mainly Brønsted acid (BA) sites often presents very limited activity towards the C-H bond activation of lower alkanes such as ethane [21]. On the other hand, BA sites are critical for the oligomerization of olefinic intermediates [22]. Thus, modification with metals has been explored to improve the catalytic performance of zeolites by enriching the Lewis acid (LA) sites or forming synergetic BA-LA pair sites [13]. Typical examples mainly include Mo, Ga, and Zn modified zeolites [23,24]. However, severe deactivation is usually observed over

Mo-based zeolites owing to significant coke formation [25,26], Ga-based zeolites typically show a relatively low activity for C1-C2 conversion [27], and Zn-based zeolites suffer from issues associated with Zn leaching under a reductive atmosphere at elevated temperatures such as 873 K [28]. Other examples, including Re, Pt, Ag, and Ni modified zeolites, usually exhibit a wide product distribution due to their strong hydrogenation capacity, which could further hydrogenate the desired aromatic products [29–32].

Our previous studies have shown that Fe-modified catalysts on CeO_2 can effectively activate the C-H bonds while protecting the C-C bond of ethane to selectively produce ethylene, which is an important intermediate for aromatization [11,33]. Fe-based catalysts have also been identified to be promising for the aromatization reaction [34]. These findings suggest a promising use of Fe to modify ZSM-5 for the aromatization of ethane. The coupling of ethane aromatization with CO_2 reduction can enhance the stability of Fe/ZSM-5 by preventing coke deposition. The current paper attempts to confirm such hypothesis and reports reactor studies and *in-situ* characterization of Fe/ZSM-5 for the simultaneous CO_2 reduction and ethane aromatization.

2. Materials and methods

2.1 Catalyst synthesis

The as-received ZSM-5 zeolite (Alfa Asear, 425 $m^2 \cdot g^{-1}$, Si/Al = 40) was pretreated in air at 823 K for 5 h before use. The Fe/ZSM-5 and Fe/CeO_2 catalysts with a Fe metal loading of 2.0 wt% were synthesized over the pretreated ZSM-5 and commercial CeO_2 (Sigma-Aldrich, 35-45 $m^2 \cdot g^{-1}$, nanopowder) supports, respectively, using the incipient wetness impregnation method described previously [14]. As a control experiment, the as-prepared Fe/CeO_2 catalyst was mechanically mixed with the pretreated ZSM-5 with a weight ratio of 1:1 to obtain the physical mixture, denoted as Fe/CeO_2+ZSM-5 (physically mixed).

2.2 Catalyst characterization

2.2.1 *In-situ* X-ray diffraction (XRD) measurements

The high-resolution synchrotron XRD patterns were collected with a wavelength of 0.39433 Å at the Beamline 17-BM of Advanced Photon Source (APS) at Argonne National Laboratory (ANL). For each *in-situ* XRD measurement, approximately 50 mg of fresh catalyst (60-80 mesh) was loaded into an amorphous silica capillary tubing mounted to a Clausen cell setup as described in the previous work [35,36]. The temperature was increased from 300 K to 873 K at a ramping rate of 20 $K \cdot min^{-1}$, during which the sample was activated in He (10 $mL \cdot min^{-1}$) for 30 min. Then a mixture of ethane/CO_2/He (3/3/4 $mL \cdot min^{-1}$) was fed into the capillary tubing and was held at 873 K for 40 min. Afterwards, it was subsequently switched to different mixtures, *i.e.*, CO_2/He (3/7 $mL \cdot min^{-1}$, 30 min) and ethane/He (3/7 $mL \cdot min^{-1}$, 30 min), so as to track the variation

of catalyst structures under different environments. The two-dimensional (2D) diffraction patterns were continuously collected by a Perkin Elmer Amorphous Silicon detector, which were subsequently integrated using the Fit2D program [37] to obtain XRD profiles. Structural refinement was performed with a Rietveld method using the GSAS software [38].

2.2.2 *In-situ* X-ray adsorption fine structure (XAFS) measurements

The *in-situ* XAFS spectra of Fe K-edge were collected at the Beamline 2-2 of Stanford Synchrotron Radiation Lightsource (SSRL). The detailed procedures for sample preparation and data collection have been previously reported [35]. The sample was first activated in He (10 $mL \cdot min^{-1}$) at 873 K for 30 min, and then the spectra were collected after the sample was cooled down to 373 K in He. Afterwards, the gas flow was switched to a mixture of ethane/CO_2/He (3/3/4 $mL \cdot min^{-1}$), and the sample was heated back to 873 K with a ramping rate of 20 $K \cdot min^{-1}$. After 85 min of reaction, the sample was cooled down to 373 K under the reactant flow to collect the XAFS spectra. The X-ray absorption near edge spectroscopy (XANES) and extended X-ray absorption fine structure (EXAFS) results were analyzed using the analysis method previously specified in Refs. [11,14].

2.2.3 Thermogravimetric analysis (TGA) measurements

Temperature programmed oxidation-thermogravimetric analysis (TPO-TGA) technique was employed to analyze the carbonaceous species deposited over the spent catalysts. The TGA measurements were performed using a Pyris Series-Diamond TG/DTA instrument with a precision of temperature measurement of ± 0.1 K and an accuracy of weight measurement of 0.01%. Procedures for TGA measurements and analyses were

described previously [13].

2.3 Catalytic performance evaluation

As illustrated in Fig. S1 in Supplementary Material (SI), the flow reactor experiments were performed in a quartz tube reactor (4.0 mm ID) under atmospheric pressure. In a typical experiment, approximately 300 mg of fresh catalyst (40-60 mesh) was loaded into the isothermal region of the reactor. The catalyst was activated in Ar (20 $mL \cdot min^{-1}$) at 873 K for 1 h prior to reaction. Then a mixture of ethane/CO_2/Ar (3/3/4 $mL \cdot min^{-1}$) was introduced into the reactor. Ar was used as the internal standard to correct the volume change due to thermal expansion and chemical reaction. Detailed procedures for the steady-state experiments are described in the SI. For the pulse reactor studies, the experiments were carried out by following the procedures previously specified in Ref. [39].

3. Results and discussion

Reactions of ethane with CO_2 were performed over Fe/ZSM-5, Fe/CeO_2 and ZSM-5 at 1 atm and 873 K. As shown in Fig. 1, the catalytic performances over different catalysts were compared at the (pseudo) steady state. It shows that Fe/ZSM-5 was the most active and selective catalyst among the three for the aromatization of ethane with CO_2, exhibiting the highest yield of benzene and toluene. The ethane conversion over Fe/ZSM-5 was almost two and five times higher than that over Fe/CeO_2 and ZSM-5, respectively. The Fe/CeO_2 catalyst only favored the ODH and DR of ethane with no aromatics being produced. The unmodified ZSM-5 exhibited comparable selectivity to benzene and toluene, but the yield of aromatics was significantly limited by its much lower activity. To explore the synergetic effect between Fe species and ZSM-5, different combinations of Fe/CeO_2 and ZSM-5 catalysts of 1:1 weight ratio were evaluated under identical conditions. As Fe/CeO_2 and ZSM-5 were separately loaded into two continuous beds, ethane was supposed to be first dehydrogenated with CO_2 to ethylene over the upstream Fe/CeO_2, which was then aromatized over the downstream ZSM-5. However, the obtained yield of aromatics was much lower compared to that over Fe/ZSM-5. Moreover, in the case of physically mixed Fe/CeO_2 and ZSM-5, the selectivity to aromatics was even lower with the dry reforming contribution being enhanced. This was most likely due to the relatively low local concentration of ethylene, making its *in-situ* aromatization difficult. The above results indicated that the synergetic effect between Fe and ZSM-5 should enhance the aromatization of ethane, which cannot be achieved by physical combinations of the catalysts. Furthermore, although a notable amount of

ethylene was produced over Fe/ZSM-5, it should be easily separated from the liquid products and recycled for further aromatization. The activity and selectivity as a function of time on stream for the five types of catalysts are shown in Fig. S2 in SI, and no obvious deactivation was observed over Fe/ZSM-5 over the duration of the experiments. To investigate the catalyst structures under reaction conditions, *in-situ* XRD measurements were performed over Fe/ZSM-5 and Fe/CeO_2. As shown in Fig. 2(a and b) and Table S1 in SI, the crystal structure of ZSM-5 at the fresh stage was refined to hold a monoclinic P21/n space group (#14) with its lattice constants being *a*=13.412 Å, *b*=20.113 Å, *c*=19.936 Å, *β*=89.88° (volume=~5378 $Å^3$). The larger zeolite cell volume measured in the Fe/ZSM-5 sample compared with the theoretical ZSM-5 (~5356.4 $Å^3$) structure was most likely due to the incorporation of Fe cations into the zeolite framework [40], as will be discussed later in the XAFS results. No reflections of Fe phases (*e.g.*, Fe_2O_3, Fe_3O_4, FeO, and Fe) were detected over Fe/ZSM-5 (Fig. 2a), suggesting their high dispersion on the zeolite surface or even incorporation into the zeolite framework. Once Fe/ZSM-5 was activated, the volume of ZSM-5 decreased rapidly to ~5358 $Å^3$ (Fig. 2b). Such a volume contraction was consistent with the gradual peak shift toward higher 2*θ* values (Fig. 2a). Under both activation and reaction conditions, the *β* angle (89.95°) became closer to 90° compared with that (88.88°) at the fresh stage, consistent with a previous report of phase transition of monoclinic ($P2_1/n$) to orthorhombic (Pnma) upon heat treatments [41]. For comparison, *in-situ* XRD results of Fe/CeO_2 are shown in Fig. 2(c). One main difference was that, although no Fe phases were detected over the fresh and activated samples, diffraction peaks of Fe_3O_4 [8.89° for(311) and 10.69° for (400)]

were observed over Fe/CeO_2 during the reaction of ethane with CO_2, indicating that the structure of Fe species over CeO_2 was different from Fe/ZSM-5. Moreover, the refinement results (Fig. 2d and Table S1 in SI) of CeO_2 retained a similar lattice volume under the conditions of activation, reaction, CO_2 only, and ethane only.

The local bonding environment of Fe species was further investigated by XAFS analysis at the Fe K-edge for both Fe/ZSM-5 and Fe/CeO_2. As shown in Fig. 3(a), the XANES features of Fe/ZSM-5 indicated that Fe was in oxidized states and the average valence of Fe remained relatively stable under reaction conditions. As shown in Fig. 3(b), EXAFS fitting was performed to probe the local environment of Fe atoms. The fitting results in Table 1 revealed that the Fe atoms in Fe/ZSM-5 formed chemical bonds with both Fe and O atoms, resulting in a Fe-Fe bond of 3.02 Å and two types of Fe-O bonds of 1.91 Å and 2.08 Å. The first Fe-O bond with a larger coordination number (CN) of 3.6 was assigned to the FeO_x clusters; in contrast, the longer Fe-O bond showed a much smaller CN (1.5) than the expected values of any Fe oxide phases, suggesting the incorporation of Fe into the ZSM-5 framework [40,42,43]. For comparison, *in-situ* XAFS results of Fe/CeO_2 were also shown in Fig. S3 in SI and summarized in Table 1. A comparison of the XANES spectra of Fe/CeO_2 before and after reaction with the reference of Fe standards suggested that a portion of Fe_2O_3 species was reduced to Fe_3O_4 during the reaction, consistent with the *in-situ* XRD results. Accordingly, the EXAFS fitting of Fe/CeO_2 after reaction showed the Fe-Fe (2.99 Å) and Fe-O (1.91 Å) bonds with a coordination number of 4.5 and 5.9, respectively.

To further understand the synergistic effect between Fe and ZSM-5, additional tests were

carried out over Fe/ZSM-5 and ZSM-5 using ethylene and CO_2 as reactants (Fig. 4). It revealed that Fe/ZSM-5 and ZSM-5 showed different catalytic performances for the reactions of CO_2 with ethane or ethylene. As compared in Fig. 4(a and c) and Table 2, Fe/ZSM-5 exhibited five times higher activity than ZSM-5 during the reaction of ethane with CO_2, but the aromatics selectivity over the two catalysts was similar. In contrast, almost identical conversions (Fig. 4b and d and Table 2) were obtained for the reactions of ethylene over the two catalysts, while the aromatics selectivity over Fe/ZSM-5 doubled that over ZSM-5. According to the *in-situ* XAFS results, the Fe species in Fe/ZSM-5 should exist in two forms, namely Fe oxides supported on the intra-/extra-pore surface of ZSM-5 and Fe cations incorporated into the ZSM-5 framework, while the Fe species in Fe/CeO_2 retained as Fe oxides. Moreover, given the catalytic performance of Fe/CeO_2 (Fig. 1), Fe oxides could only activate hydrocarbons instead of directly catalyzing the aromatization reaction of either ethane or ethylene. Thus, the increased selectivity in the step of ethylene aromatization over Fe/ZSM-5 should be caused by the incorporated Fe cations, while the enhanced activation of ethane was most likely contributed by both the supported Fe oxides and the incorporated Fe cations.

Reactions of ethane with and without CO_2 were carried out in both flow reactor and pulse reactor to investigate the effect of CO_2. The flow reactor results in Fig. 5 showed that when CO_2 was present, both the ethane conversion and aromatics selectivity over Fe/ZSM-5 were significantly decreased, while the stability and C_2H_4 selectivity were noticeably enhanced. In comparison, the effect of CO_2 on ZSM-5 and Fe/CeO_2 was relatively weak. The inhibition effect of CO_2 on ethane conversion and aromatization over

Fe/ZSM-5 was potentially due to dealumination or modification of acid sites over Fe cations by the water vapor *in-situ* generated from RWGS [44–46]. In order to gain more insights into the inhibition effect, pulse reactor experiments were carried out as shown in Fig. S4 in SI. The results indicated that the introduction of CO_2 could significantly promote the dry reforming pathway, thereby decreasing the concentration of ethylene and consequently against the aromatization reaction. It has been reported that steam would transfer the LA sites derived from the metal modifiers (*e.g.*, Ga and Zn) to a less active BA sites, thereby decreasing the aromatization capacity of catalysts [13,45,47]. To further verify this speculation, additional tests were carried out by injecting CO_2 and H_2O intermittently into the feed streams. As shown in Fig. 6, when CO_2 was injected into the reaction system, a small amount of water was detected, leading to an obvious decrease in both ethane conversion and aromatics yield, but the aromatization of ethane could largely recover to its initial level after removing CO_2. Likewise, the addition of water decreased the production of aromatics, and it was also a reversible process. These results proved that the negative effect of CO_2 on ethane aromatization over Fe/ZSM-5 should be dominated by the formation of water rather than dealumination. Therefore, further work is needed to identify more water-tolerant zeolite catalysts to better combine ethane aromatization with CO_2 reduction. One way to improve the water tolerance and consequently the aromatics yield is by modifying the catalysts with P, as recently demonstrated in the utilization of P-modified Ga/ZSM-5 for the reaction of ethane and CO_2 [13]. It should be noted that the conversion versus time plots in Fig. 5 and Fig. S2 in SI revealed that CO_2 could help improve the catalyst stability, likely by removing coke via

the reverse Boudouard reaction. The type and quantity of carbon deposits on the spent Fe/ZSM-5 catalyst with and without CO_2 were studied by TPO-TGA (Fig. 7), showing that the coke formation was significantly suppressed with the presence of CO_2. Compared with the previous reported Ga/ZSM-5 catalyst [13], Fe/ZSM-5 exhibited a more stable feature despite its lower activity than the former. The TGA results (Fig. S5 in SI) of the spent Fe/CeO_2 and Fe/ZSM-5 catalysts also indicated a positive effect of CO_2 on the elimination of coke formation.

4. Conclusions

In the present work, Fe/ZSM-5 has been identified as a promising catalyst for the direct production of aromatics from CO_2-assisted ethane aromatization. The comparison of Fe/ZSM-5 with Fe/CeO_2, ZSM-5, and their physical mixtures indicated that the synergetic effect between Fe and ZSM-5 contributed to an enhanced activity for aromatization. The structural information of Fe/ZSM-5 was revealed by *in-situ* XRD and XAFS analysis, suggesting that the Fe species mainly existed in two forms, *i.e.*, the extra-framework Fe oxides and the Fe cations incorporated into the zeolite framework. The dehydrogenation of ethane was executed by both the extra-framework Fe oxides and the incorporated Fe cations, while ethylene aromatization over Fe/ZSM-5 should be promoted by the incorporated Fe cations. Although the presence of CO_2 reduced ethane conversion and aromatics selectivity due to the reversible modification of acid sites by steam *in-situ* formed from the RWGS reaction, the Fe/ZSM-5 catalyst showed higher stability during the reaction with the assistance of CO_2 for coke resistance. Additional research should be explored to enhance the steam tolerance of zeolites to take

advantage of the tandem reaction of CO_2-assisted ethane dehydrogenation and aromatization to generate liquid products of higher value from the abundant shale gas while achieving the simultaneous reduction of greenhouse gas CO_2.

Acknowledgment

Authors at Columbia University and Brookhaven National Laboratory acknowledge financial support from the US Department of Energy, Basic Energy Sciences, Catalysis Science Program under contract number DE-SC0012704. The *in-situ* data were collected with help from the Synchrotron Catalysis Consortium under the grant number DE-FG02-05ER15688.

Declaration of competing interest

The authors declare no competing interests.

References

[1] K.O. Yoro, M.O. Daramola, in: M.R. Rahimpour, M. Farsi, M.A. Makarem (Eds.), Advances in Carbon Capture, Woodhead Publishing, 2020: pp. 3–28.

[2] United Nations, Climate Change, Communication of long-term strategies, https://unfccc.int/process/the-paris-agreement/long-term-strategies (accessed April 2, 2021).

[3] P. Gabrielli, M. Gazzani, M. Mazzotti, Ind. Eng. Chem. Res. 59 (2020) 7033–7045.

[4] D.Y.C. Leung, G. Caramanna, M.M. Maroto-Valer, Renew. Sustain. Energy Rev. 39 (2014) 426–443.

[5] B.M. Tackett, E. Gomez, J.G. Chen, Nat. Catal. 2 (2019) 381–386.

[6] D. Wang, Z. Xie, M.D. Porosoff, J.G. Chen, Chem (2021), in press.

[7] Z. Xie, L.R. Winter, J.G. Chen, Matter 4 (2021) 408–440.

[8] Z. Xie, E. Gomez, J.G. Chen, AIChE J. (2021) e17249.

[9] A. Rafiee, K. Rajab Khalilpour, D. Milani, M. Panahi, J. Environ. Chem. Eng. 6 (2018) 5771–5794.

[10] Y.Y. Birdja, E. Pérez-Gallent, M.C. Figueiredo, A.J. Göttle, F. Calle-Vallejo, M.T.M. Koper, Nat. Energy 4 (2019) 732–745.

[11] Z. Xie, D. Tian, M. Xie, S.-Z. Yang, Y. Xu, N. Rui, J.H. Lee, S.D. Senanayake, K. Li, H. Wang, S. Kattel, J.G. Chen, Chem 6 (2020) 2703–2716.

[12] Z. Xie, Y. Xu, M. Xie, X. Chen, J.H. Lee, E. Stavitski, S. Kattel, J.G. Chen, Nat. Commun. 11 (2020) 1887.

[13] E. Gomez, X. Nie, J.H. Lee, Z. Xie, J.G. Chen, J. Am. Chem. Soc. 141 (2019) 17771–17782.

[14] B. Yan, S. Yao, S. Kattel, Q. Wu, Z. Xie, E. Gomez, P. Liu, D. Su, J.G. Chen, Proc. Natl. Acad. Sci. USA. 115 (2018) 8278.

[15] J. Hiller, U.S. natgas glut dims outlook for big producers as prices head to 25-year low, 2019. https://www.reuters.com/article/us-usa-naturalgas-chesapeake-energy-idUSKBN1X92AN (accessed April 2, 2021).

[16] M.D. Porosoff, M.N.Z. Myint, S. Kattel, Z. Xie, E. Gomez, P. Liu, J.G. Chen, Angew. Chem. Int. Ed. 54 (2015) 15501–15505.

[17] S. Ebrahimian, D. Iranshahi, Int. J. Hydrog. Energy 45 (2020) 19405–19419.

[18] M.R. Rahimpour, M. Jafari, D. Iranshahi, Appl. Energy 109 (2013) 79–93.

[19] E.A. Uslamin, H. Saito, Y. Sekine, E.J.M. Hensen, N. Kosinov, Catal. Today 369 (2020), 184-192.

[20] C. Zhang, G. Kwak, H.-G. Park, K.-W. Jun, Y.-J. Lee, S.C. Kang, S. Kim, Microporous Mesoporous Mater. 276 (2019) 292–301.

[21] Y. Ono, H. Nakatani, H. Kitagawa, E. Suzuki, in: T. Inui (Eds.), Studies in Surface Science and Catalysis, Elsevier, 1989: pp. 279–290.

[22] E.A. Uslamin, H. Saito, N. Kosinov, E. Pidko, Y. Sekine, E.J.M. Hensen, Catal. Sci. Technol. 10 (2020) 2774–2785.

[23] H. Saito, Y. Sekine, RSC Adv. 10 (2020) 21427–21453.

[24] D. Kiani, S. Sourav, Y. Tang, J. Baltrusaitis, I.E. Wachs, Chem. Soc. Rev. 50 (2021)

1251–1268.
[25] Y. Xu, L. Lin, Appl. Catal. A-Gen. 188 (1999) 53–67.
[26] J.J. Spivey, G. Hutchings, Chem. Soc. Rev. 43 (2014) 792–803.
[27] A. Bhan, W. Nicholas Delgass, Catal. Rev. 50 (2008) 19–151.
[28] J.A. Biscardi, G.D. Meitzner, E. Iglesia, J. Catal. 179 (1998) 192–202.
[29] P. Meriaudeau, C. Naccache, J. Catal. 157 (1995) 283–288.
[30] A. Krogh, A. Hagen, T.W. Hansen, C. Hviid Christensen, I. Schmidt, Catal. Commun. 4 (2003) 627–630.
[31] Y. Ono, K. Osako, G.-J. Kim, Y. Inoue, in: J. Weitkamp, H.G. Karge, H. Pfeifer, W. Hölderich (Eds.), Studies in Surface Science and Catalysis, Elsevier, 1994: pp. 1773–1780.
[32] S. Fadaeerayeni, J. Shan, E. Sarnello, H. Xu, H. Wang, J. Cheng, T. Li, H. Toghiani, Y. Xiang, Appl. Catal. A-Gen. 601 (2020) 117629.
[33] M. Myint, B. Yan, J. Wan, S. Zhao, J.G. Chen, J. Catal. 343 (2016) 168–177.
[34] X. Guo, G. Fang, G. Li, H. Ma, H. Fan, L. Yu, C. Ma, X. Wu, D. Deng, M. Wei, D. Tan, R. Si, S. Zhang, J. Li, L. Sun, Z. Tang, X. Pan, X. Bao, Science 344 (2014) 616-619.
[35] B. Yan, X. Yang, S. Yao, J. Wan, M. Myint, E. Gomez, Z. Xie, S. Kattel, W. Xu, J.G. Chen, ACS Catal. 6 (2016) 7283–7292.
[36] P.J. Chupas, K.W. Chapman, C. Kurtz, J.C. Hanson, P.L. Lee, C.P. Grey, J. Appl. Crystallogr. 41 (2008) 822–824.
[37] A.P. Hammersley, S.O. Svensson, M. Hanfland, A.N. Fitch, D. Hausermann, High Press. Res. 14 (1996) 235–248.
[38] B.H. Toby, J. Appl. Crystallogr. 34 (2001) 210–213.
[39] Z. Xie, B. Yan, J.H. Lee, Q. Wu, X. Li, B. Zhao, D. Su, L. Zhang, J.G. Chen, Appl. Catal. B-Environ. 245 (2019) 376–388.
[40] E.A. Urquieta-González, L. Martins, R.P.S. Peguin, M.S. Batista, Mat. Res. 5 (2002) 321–327.
[41] M. Ardit, A. Martucci, G. Cruciani, J. Phys. Chem. C. 119 (2015) 7351–7359.
[42] P. Marturano, L. Drozdová, A. Kogelbauer, R. Prins, J. Catal. 192 (2000) 236–247.
[43] E. Yuan, G. Wu, W. Dai, N. Guan, L. Li, Catal. Sci. Technol. 7 (2017) 3036–3044.
[44] A.P. Hawkins, A. Zachariou, S.F. Parker, P. Collier, N. Barrow, I.P. Silverwood, R.F. Howe, D. Lennon, RSC Adv. 10 (2020) 23136–23147.
[45] A. Mehdad, N.S. Gould, B. Xu, R.F. Lobo, Catal. Sci. Technol. 8 (2018) 358–366.
[46] J. Holzinger, P. Beato, L.F. Lundegaard, J. Skibsted, J. Phys. Chem. C. 122 (2018) 15595–15613.
[47] H. Fan, X. Nie, H. Wang, M.J. Janik, C. Song, X. Guo, Catal. Sci. Technol. 10 (2020) 8359–8373.

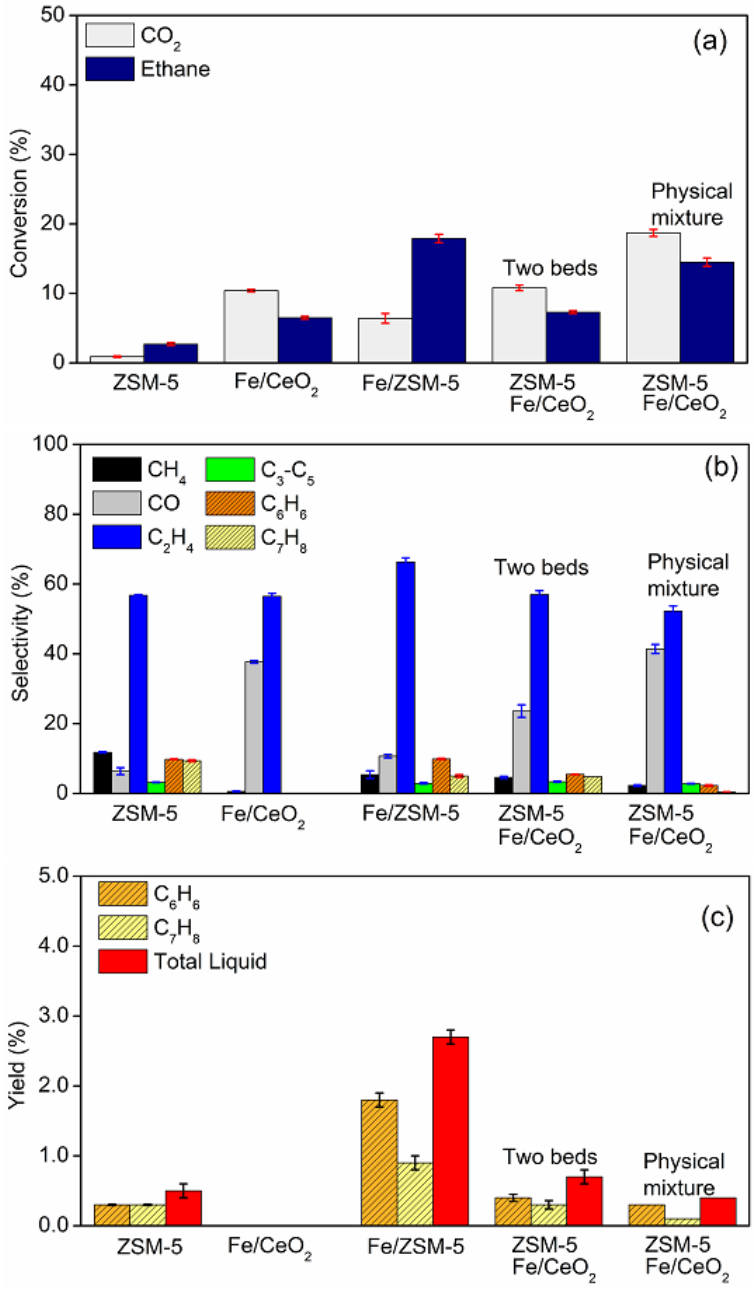

Fig. 1. Catalytic performance of different catalysts for CO_2-assisted ethane aromatization in a flow reactor. (a) Conversion of ethane, (b) product selectivity (ethane-based), and (c) yield of aromatics at the (pseudo) steady state. Reaction conditions: 300 mg of Fe/ZSM-5, Fe/CeO_2 or ZSM-5, and 600 mg of Fe/CeO_2 + ZSM-5 (loaded in two continuous beds, weight ratio of 1:1) and Fe/CeO_2 + ZSM-5 (physically mixed, weight ratio of 1:1) at 1 atm, 873 K, ethane/CO_2/Ar = 3/3/4 mL·min^{-1}.

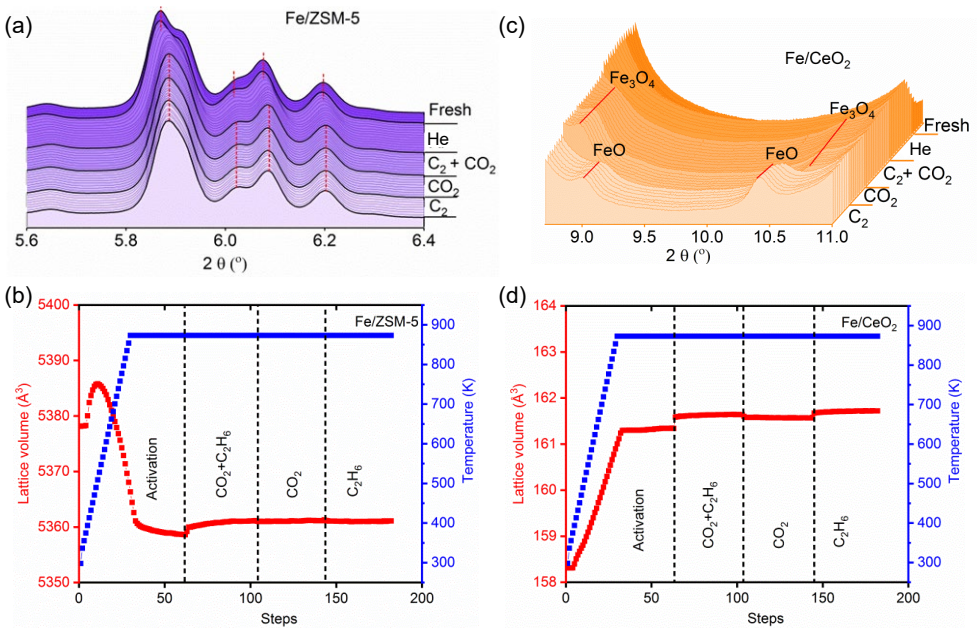

Fig. 2. *In-situ* XRD profiles and lattice refinements of Fe/ZSM-5 and Fe/CeO_2. (a) and (c) are the *in-situ* XRD profiles of Fe/ZSM-5 and Fe/CeO_2, respectively, under the fresh (300 K), activation (Ar, 873 K), reaction (C_2+CO_2, 873 K), CO_2 only (873 K), and ethane only (873 K) conditions. (b) and (d) refer to the variation of lattice volume of the ZSM-5 and CeO_2 support, respectively, at different reaction stages.

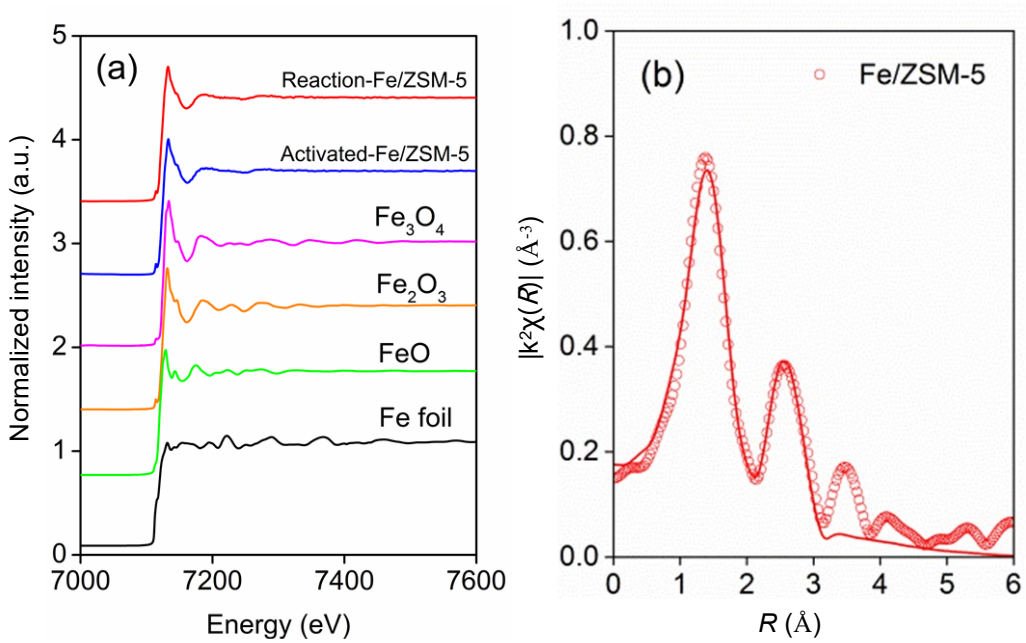

Fig. 3. *In-situ* XAFS results of Fe/ZSM-5. (a) refers to the XANES spectra of Fe K-edge of Fe/ZSM-5 (after activation and reaction); for comparison, metal and metal oxide standards were also demonstrated; (b) illustrates the EXAFS fitting results of Fe K-edge in R space for Fe/ZSM-5 under the reaction condition.

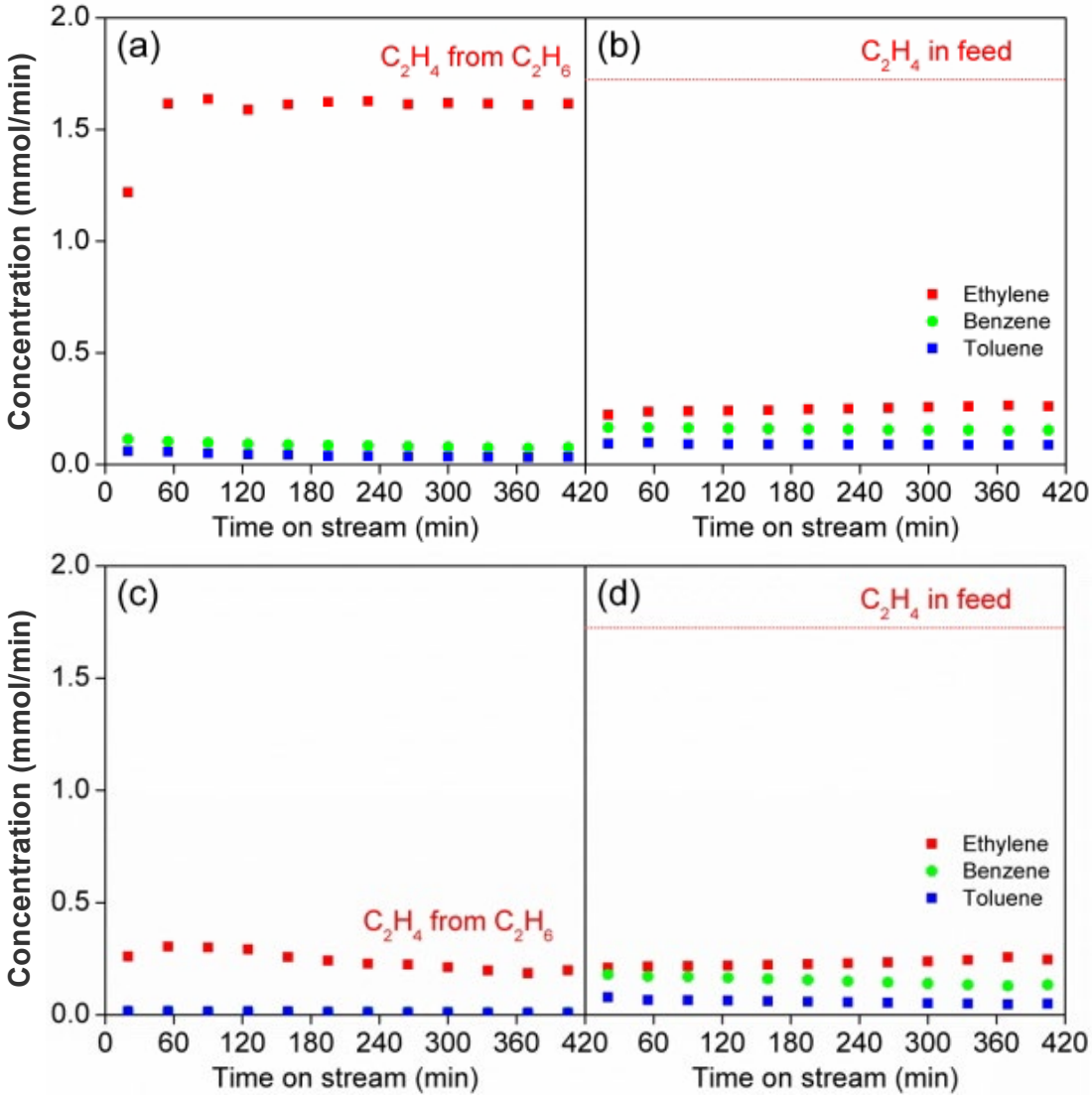

Fig. 4. Comparison of reactions of CO_2 with ethane and with ethylene. (a) and (b): Fe/ZSM-5; (c) and (d): ZSM-5. Reaction conditions: 1 atm, 873 K, $C_2H_6/CO_2/Ar$ = 3/3/4 mL·min^{-1} or $C_2H_4/CO_2/Ar$ = 0.5/3.0/6.5 mL·min^{-1}, catalyst of 300 mg; for a better comparison, the concentration of C_2H_4 in the reactions of C_2H_4 with CO_2 was kept similar to the concentration of C_2H_4 produced from C_2H_6 in the reactions of C_2H_6 with CO_2.

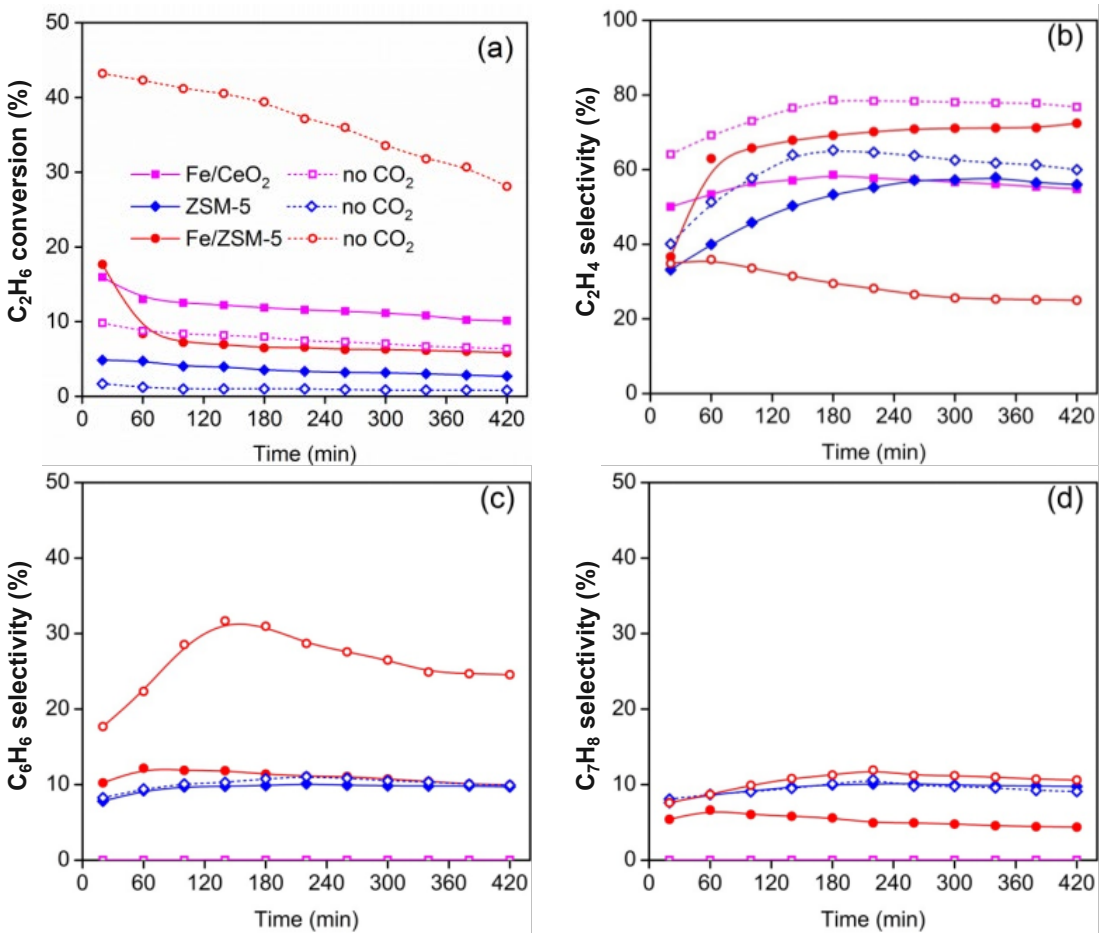

Fig. 5. Effect of CO_2 on the catalytic performance over Fe/ZSM-5, ZSM-5 and Fe/CeO_2. (a) refers to the conversion of ethane with and without CO_2 as a function of time on stream; (b)-(d) are the selectivity to ethylene, benzene and toluene as a function of time on stream, respectively. Reaction conditions: 1 atm, 873 K, $C_2H_6/CO_2/Ar$ = 3/3/4 mL·min^{-1} or C_2H_6/Ar = 3/7 mL·min^{-1}, catalyst of 300 mg.

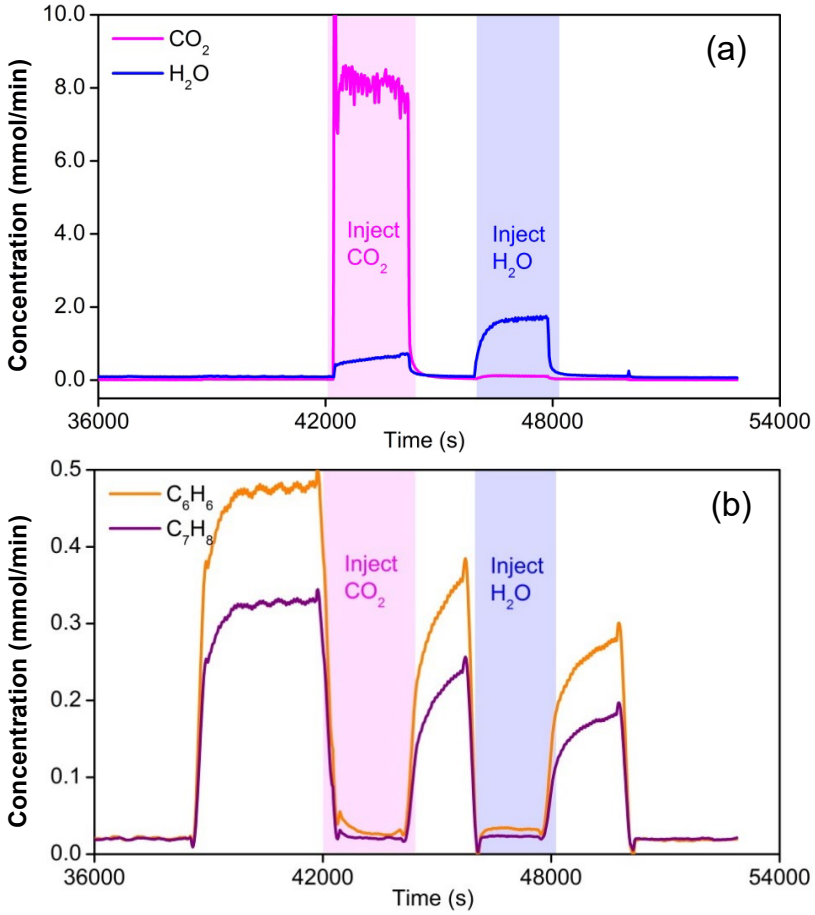

Fig. 6. Ethane aromatization over Fe/ZSM-5 with intermittent injections of CO_2 and water vapor. (a) displays the concentration of CO_2 and H_2O as a function of time; (b) illustrates the plots of concentration of benzene and toluene during the same period of (a). Reaction conditions: C_2H_6 (10 mL·min^{-1}) with CO_2 (1 mL·min^{-1}) or C_2H_6 (10 mL·min^{-1}) with water of the saturated vapor pressure at 873 K and 1 atm. The concentrations of ethane, benzene and toluene as well as the CO_2 and H_2O signals were continuously collected by a SRS residual gas analyzer.

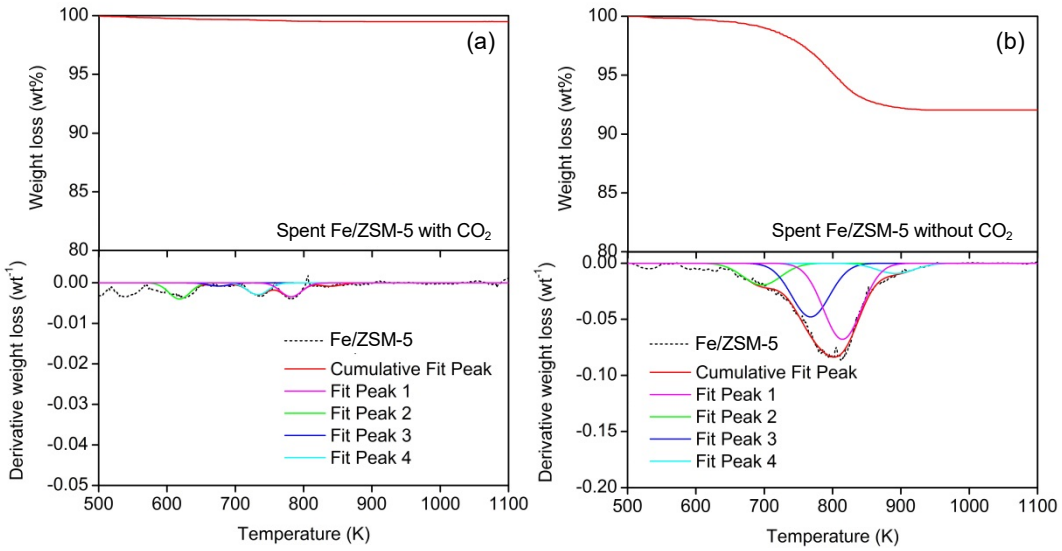

Fig. 7. TPO-TGA and DTG characterization of the spent Fe/ZSM-5 catalyst with CO_2 (a) and without CO_2 (b).

Table 1. EXAFS fitting results for Fe/ZSM-5 and Fe/CeO_2 under reaction conditions of ethane with CO_2 at 873 K.

Catalysts	Shell	*CN*	*R* (Å)	σ^2 (Å^2)	E_0 shift (eV)
Fe/ZSM-5	Fe-O	3.6±0.3	1.91±0.02	0.011	2.5
	Fe-O	1.5±0.5	2.08±0.02	0.011	
	Fe-Fe	6.5±2.1	3.02±0.01	0.024	
Fe/CeO_2	Fe-O	5.9±0.7	1.93±0.01	0.013	-3.6
	Fe-Fe	4.5±1.5	2.99±0.01	0.019	

Notes: *CN* is the averaged coordination number; *R* is bond length; σ^2 is the mean square variation in the path length.

Table 2. Comparison between reactions of CO_2 with ethane and with ethylene over Fe/ZSM-5 and ZSM-5.

Catalysts	Gas Feeds[a] (mL·min^{-1})				Conversion[b] (%)		Selectivity[b] (%)	
	C_2H_6	C_2H_4	CO_2	Ar	CH	CO_2	C_6H_6	C_7H_8
Fe/ZSM-5	-	0.5	0.5	9.0	60.8	6.1	46.5	26.4
Fe/ZSM-5	3.0	-	3.0	4.0	17.9	6.4	9.9	5.0
ZSM-5	-	0.5	0.5	9.0	59.8	8.4	33.0	12.1
ZSM-5	3.0	-	3.0	4.0	2.7	0.9	9.8	9.4

[a]: 1 atm, 873 K, total flow rate of 10 mL·min^{-1}, catalyst of 300 mg; the concentration of C_2H_4 in the reactions of C_2H_4 with CO_2 was kept similar to that produced from the reactions of C_2H_6 with CO_2;

[b]: conversion and selectivity were obtained at the (pseudo) steady state after time on stream for 5 h.